



# Seasonal temperature response over the Indochina Peninsula to a worst-case high-emission forcing: a study with the regionally coupled model ROM

Shoupeng Zhu<sup>1,3,5</sup> · Fei Ge<sup>2,3,5</sup> · Frank Sielmann<sup>4</sup> · Mengting Pan<sup>1,5</sup> · Klaus Fraedrich<sup>1,3</sup> · Armelle Reça C. Remedio<sup>6</sup> · Dmitry V. Sein<sup>7</sup> · Daniela Jacob<sup>6</sup> · Hao Wang<sup>8</sup> · Xiefei Zhi<sup>1,5</sup>

Received: 21 November 2019 / Accepted: 23 July 2020  
© Springer-Verlag GmbH Austria, part of Springer Nature 2020

## Abstract

Changes of surface air temperature (SAT) over the Indochina Peninsula (ICP) under the Representative Concentration Pathway (RCP) 8.5 scenario are projected for wet and dry seasons in the short-term (2020–2049) and long-term (2070–2099) future of the twenty-first century. A first analysis on projections of the SAT by the state-of-the-art regionally coupled atmosphere-ocean model ROM, including exchanges of momentum, heat, and water fluxes between the atmosphere (Regional Model) and ocean (Max Planck Institute Ocean Model) models, shows the following results: (i) In both seasons, the highest SAT occurs over the southern coastal area while the lowest over the northern mountains. The highest warming magnitudes are located in the northwestern part of the ICP. The regionally averaged SAT over the ICP increases by 2.61 °C in the wet season from short- to long-term future, which is slightly faster than that of 2.50 °C in the dry season. (ii) During the short-term future, largest SAT trends occur over the southeast and northwest ICP in wet and dry seasons, respectively. On regional average, the wet season is characterized by a significant warming rate of 0.22 °C decade<sup>-1</sup>, while it is non-significant with 0.11 °C decade<sup>-1</sup> for the dry season. For the long-term future, the rapid warming is strengthened significantly over whole ICP, with trends of 0.51 °C decade<sup>-1</sup> and 0.42 °C decade<sup>-1</sup> in wet and dry seasons, respectively. (iii) In the long-term future, more conspicuous warming is noted, especially in the wet season, due to the increased downward longwave radiation. Higher CO<sub>2</sub> concentrations enhancing the greenhouse effect can be attributed to the water vapor-greenhouse feedback, which, affecting atmospheric humidity and counter radiation, leads to the rising SAT.

## 1 Introduction

Latest observational records confirmed the warming trends of the surface air temperature (SAT) in most countries of Southeast Asia during the past few decades (IPCC 2013). Correspondingly, the frequency and intensity of high

temperature extremes have increased over this region (Manton et al. 2001; Tangang et al. 2007; IPCC 2014; Ngo-Duc et al. 2017). In addition, the local economy of Southeast Asia significantly relies on agriculture and forestry, which are highly vulnerable to climate change. The Indochina Peninsula (ICP), located between the western Pacific and the Indian

✉ Fei Ge  
figo@cuit.edu.cn

✉ Xiefei Zhi  
zhi@nuist.edu.cn

<sup>1</sup> Collaborative Innovation Center on Forecast and Evaluation of Meteorological Disasters/Key Laboratory of Meteorological Disasters, Ministry of Education, Nanjing University of Information Science & Technology, Nanjing, China

<sup>2</sup> School of Atmospheric Sciences/Plateau Atmosphere and Environment Key Laboratory of Sichuan Province/Joint Laboratory of Climate and Environment Change, Chengdu University of Information Technology, Chengdu, China

<sup>3</sup> Max Planck Institute for Meteorology, Hamburg, Germany

<sup>4</sup> Meteorological Institute, University of Hamburg, Hamburg, Germany

<sup>5</sup> WeatherOnline Institute of Meteorological Applications, Wuxi, China

<sup>6</sup> Climate Service Center Germany, Helmholtz Centre for Materials and Coastal Research, Hamburg, Germany

<sup>7</sup> Alfred Wegener Institute, Helmholtz Centre for Polar and Marine Research, Bremerhaven, Germany

<sup>8</sup> College of Atmospheric Sounding, Chengdu University of Information Technology, Chengdu, China

Ocean, is generally considered a representative monsoon region. With a large coastal population in complex terrains exposed to weather and climate extremes, it is of great importance to investigate the possible impacts of future climate changes and, especially for the surrounding developing countries, to implement adaptation measures for risk reduction (Karl and Easterling 1999; Schleussner et al. 2016; Holden et al. 2018; Ge et al. 2019b). So far, many studies have improved the understanding of the present climate variability of the ICP (Takahashi and Yasunari 2006; Hsu et al. 2014; Villafuerte and Matsumoto 2015; Ge et al. 2017; Ge et al. 2019a). However, the information associated with projected changes of the future climate is still missing for the Indochina Peninsula region on either CMIP5 ensembles or regional high-resolution climate simulations.

Currently, it is necessary to acknowledge the potential risks of a warming climate over the ICP, especially under the worst scenario assumption, characterized by the Representative Concentration Pathway (RCP) 8.5 (IPCC 2018). This scenario corresponds to the highest CO<sub>2</sub> emissions pathway, which is a so-called baseline scenario that does not include any specific climate mitigation target (Riahi et al. 2011). The projected climate changes under the RCP 8.5 scenario do not only provide essential information to manageable climate adaptation and mitigation strategies for the developing countries in ICP but also highlight the importance to restrict the global warming to 1.5 °C guided by the Paris Agreement (UNFCCC 2015).

It has been generally recognized that global and regional climate models (GCMs and RCMs) supplement one another as effective tools to investigate climate and climate change. Additionally, various ecological and societal problems associated with climate change in the context of global warming have been addressed over the past decades (IPCC 2013). To satisfy the increasing demand of understanding future climate evolution, climate research communities have been accelerating the development of models (Giorgi et al. 2009; Moss et al. 2010). For instance, the Coupled Model Intercomparison Project Phase 3 (CMIP3) and Phase 5 (CMIP5) involve more than 20 climate modeling groups, which publicly provide a number of coordinated climate model experiments towards the future climate change projections (Meehl et al. 2007; Taylor et al. 2012). However, historically, due to the restriction of the computational capability, GCMs were limited to climate investigations with insufficient horizontal resolutions, which tend to produce large uncertainties and discrepancies in climate simulations and projections. Therefore, the RCMs with advanced parameterizations and dynamically downscaled climate information have been increasingly applied to investigate the regional climates of interest (Aldrian et al. 2005; Giorgi 2006; Feser et al. 2011; Sein et al. 2014; Cabos et al. 2017; Ge et al. 2019b).

The regionally coupled atmosphere-ocean model ROM (Regional Model (REMO)-Ocean Atmosphere Sea Ice Soil (OASIS)-Max Planck Institute Ocean Model (MPIOM); Sein et al. 2015) has been developed and applied to study regional climate and local processes with a fairly high resolution. It divides the global ocean model MPIOM setup into two subdomains: a limited high-resolution area where the coupling takes place and the air-sea fluxes are interacting with the regional atmospheric model REMO, and elsewhere, the MPIOM is driven by prescribed atmospheric forcing with a relatively coarse resolution. This model setup aims to reduce the influence of the lateral boundary conditions, which has been demonstrated as an effective approach in ROM (Sein et al. 2014). Recent studies show the high-resolution ROM model has been indicated sufficient in regional climate representations (Gaertner et al. 2018; Zhu et al. 2020b) and widely applied to investigate the climate change and the mechanisms (Cabos et al. 2019). In this paper, ROM is employed to analyze how much the ICP region tends to warm in the twenty-first century under the worst-case high-emission scenario, thereby quantifying the expected range of temperature response over the ICP and elucidating some of its underlying mechanisms.

This paper is organized as follows: A brief model description and the methods of analysis are described in Section 2. In Section 3, we show the basic model validation results. Afterwards, the projected temperature changes covering the region from 6° N to 23° N and from 95° E to 110° E under the RCP 8.5 scenario are analyzed in the same section. Finally, the conclusions and discussions follow in Section 4.

## 2 Datasets and methodology

### 2.1 Model design

The regional coupled atmosphere-ocean-sea-ice model ROM comprises the atmospheric Regional Model (REMO; Jacob 2001; Jacob et al. 2001), the Max Planck Institute Ocean Model (MPIOM; Marsland et al. 2003; Jungclaus et al. 2013), and the Hydrological Discharge model (HD; Hagemann and Dümenil 1997; Hagemann and Gates 2001). In global configuration, the MPIOM model is run with relatively high horizontal resolution in Southeast Asia, while the HD model has a constant resolution of 0.5° × 0.5° over the globe. The atmospheric model REMO domain covers the entire area of Southeast Asia (Fig. 1a) using a rotated grid with the horizontal resolution of about 50 km (~0.5°). The models are coupled by the Ocean Atmosphere Sea Ice Soil Version 3 (OASIS3) coupler with a 3-h interval (Valcke et al. 2003). Since the regional climate REMO model only covers a specific domain of the global ocean, the ocean model MPIOM needs to be run in both coupled and standalone models

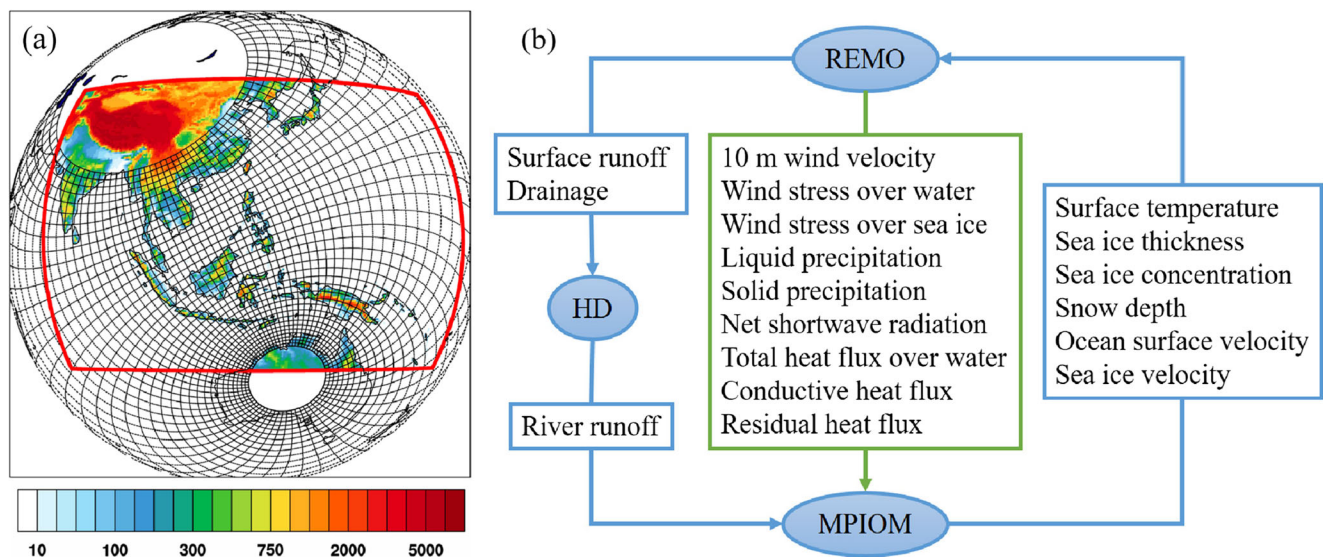


**Fig. 1** **a** Model grid configuration and orography (unit: m). Red rectangle denotes the coupled area (REMO domain). Black lines represent the MPIOM grid (every 12th grid line is shown). **b** Model coupling scheme in the coupled area

simultaneously. In the uncoupled domain, MPIOM calculates heat, freshwater, and momentum fluxes from the global, predefined atmosphere, while in the coupled area, MPIOM receives the heat, freshwater, and momentum fluxes from REMO, and transmits the sea surface conditions to the atmospheric model REMO (Fig. 1b) (for more details on the coupling, see Sein et al. 2015).

The model spin-up is divided into two phases. Firstly, the ocean model MPIOM is run in standalone mode starting from the Polar Science Center Hydrographic Climatology (Steele et al. 2001) and forced by ERA-40 reanalysis data for a 45-year period of 1958–2002. This period is performed cyclically twice and, therefore, the total spin-up for MPIOM in standalone mode is 90 years. In the second phase, the spin-up for the coupled model is forced for additional 78 years, including the 45-year period of 1958–2002 with ERA-40 reanalysis data and the 33-year period of 1980–2012 with ERA-Interim reanalysis data. After completing the spin-up process, the historical simulation is started from 1950. Following the Intergovernmental Panel on Climate Change (IPCC) Fifth Assessment Report (AR5), the radiative forcing trajectories under the RCP 8.5 (Moss et al. 2010) are applied for the atmospheric CO<sub>2</sub> concentrations in the scenario run from 2006 to 2099, representing a forcing of 8.5 W m<sup>-2</sup> by the end of twenty-first century.

## 2.2 Datasets

The CMIP5 project (<http://cmip-pcmdi.llnl.gov/cmip5/index.html>) is a collaborative framework designed by the World Climate Research Programme (WCRP) to improve knowledge of climate change, containing a series of ocean-atmosphere coupled GCMs. The model simulations under

the CMIP5 framework have been widely used to investigate both the historical and future climate and to support national and international assessments regarding climate change on the globe or some specific regions. The 38 available simulations under the RCP 8.5 from CMIP5 models (Table 1) are applied in this study as references of the general capability of ROM to project the future SAT changes over the ICP.

## 2.3 Trend calculation

Climatological trends are detected for the temperature simulations by using the Mann-Kendall test (Mann 1945; Kendall 1975) and Sen's slope estimates (Sen 1968). The methods have been widely used to quantify trends in hydro-meteorological time series and climate variability, which does not require the residuals about the fitted line to be normally distributed (Yue and Hashino 2003; Tao et al. 2011; You et al. 2013, 2015; Zhu et al. 2016). The climatological means and trends are identified for the periods of 2020–2049 (short-term future) and 2050–2099 (long-term future). Generally, the ICP experiences a wet season from April to September and a dry season from October to the subsequent March, which are applied as the seasonal classification in this study.

## 3 Results

### 3.1 Model validations for the future climate

The 38 CMIP5 simulations under the RCP 8.5 are employed to evaluate the projected SAT of the ROM model from the respect of regional average. Variations of the projected annual

**Table 1** Brief information of the used 38 CMIP5 GCMs

GCM	Institution	GCM	Institution
BCC-CSM1-1	BCC	MIROC-ESM-CHEM	MIROC
BCC-CSM1-1-M	BCC	HadGEM2-CC	MOHC
BNU-ESM	BNU	HadGEM2-ES	MOHC
CanESM2	CCCma	MPI-ESM-LR	MPI-M
CMCC-CM	CMCC	MPI-ESM-MR	MPI-M
CMCC-CMS	CMCC	MRI-CGCM3	MRI
CNRM-CM5	CNRM-CERFACS	GISS-E2-H	NASA-GISS
ACCESS1-0	CSIRO-BOM	GISS-E2-H-CC	NASA-GISS
ACCESS1-3	CSIRO-BOM	GISS-E2-R	NASA-GISS
CSIRO-Mk3-6-0	CSIRO-QCCCE	GISS-E2-R-CC	NASA-GISS
FIO-ESM	FIO	CCSM4	NCAR
EC-EARTH	ICHEC	NorESM1-M	NCC
INMCM4	INM	HadGEM2-AO	NIMR-KMA
IPSL-CM5A-LR	IPSL	GFDL-CM3	NOAA-GFDL
IPSL-CM5A-MR	IPSL	GFDL-ESM2G	NOAA-GFDL
IPSL-CM5B-LR	IPSL	GFDL-ESM2M	NOAA-GFDL
FGOALS-g2	LASG-IAP	CESM1-BGC	NSF-DOE-NCAR
MIROC5	MIROC	CESM1-CAM5	NSF-DOE-NCAR
MIROC-ESM	MIROC	CESM1-WACCM	NSF-DOE-NCAR

SAT averaged over the ICP from ROM and from the CMIP5 models are presented for the period of 2006–2099 in Fig. 2. Generally, the projected SAT of ROM varies within the range of CMIP5 simulations, which is fairly close to the CMIP5 ensemble means. The ROM projected SAT over the ICP performs similarly as the ensemble mean, with a correlation coefficient and root mean square error of 0.94 and 0.48 °C, which reveal good agreements between ROM and the CMIP5 models. Moreover, the ROM and CMIP5 ensemble mean values are characterized by similar increasing trends of SAT from 2006 to 2099 with 0.45 °C decade<sup>-1</sup> and 0.44 °C decade<sup>-1</sup>, respectively. Therefore, it is reasonable to apply ROM in projecting the regional SAT changes over the ICP, as well as to investigate the possible mechanisms responsible for the changes.

### 3.2 Projections of the surface air temperature over the ICP

The ROM projections are examined under the RCP 8.5 scenario focusing on different seasons (wet and dry) during different periods (short- and long-term future). The spatial distributions of the projected SATs and the SAT trends are depicted in Figs. 3 and 4, with the following results being obtained.

Projected spatial distributions of the SAT mean for wet and dry seasons exhibit similar patterns in the short- and long-term future, with the highest SAT located in the southern coastal area and the lowest SAT in the northern mountainous area of the ICP. The regionally averaged SATs over the ICP are 26.70 °C and 29.31 °C for the wet season in the short- and long-term future, while 22.35 °C and 24.85 °C for the dry

**Fig. 2** Plume plot of the projected annual mean SAT (unit: °C) averaged over the ICP under RCP 8.5 scenario for the period of 2006–2099, derived from the ROM model (blue bold line), the CMIP5 models (gray solid lines), and the CMIP5 ensemble mean (red bold line)

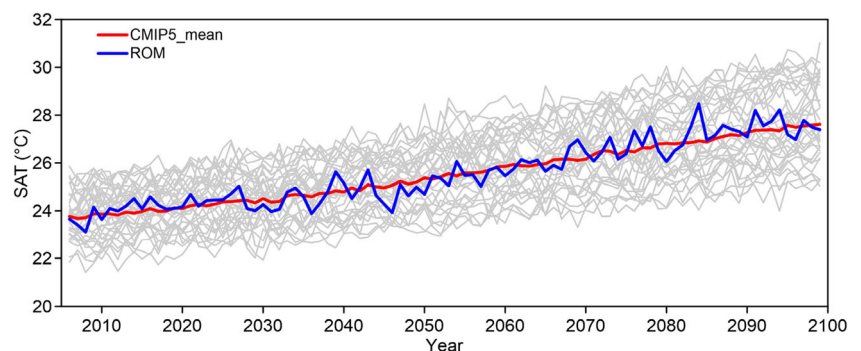
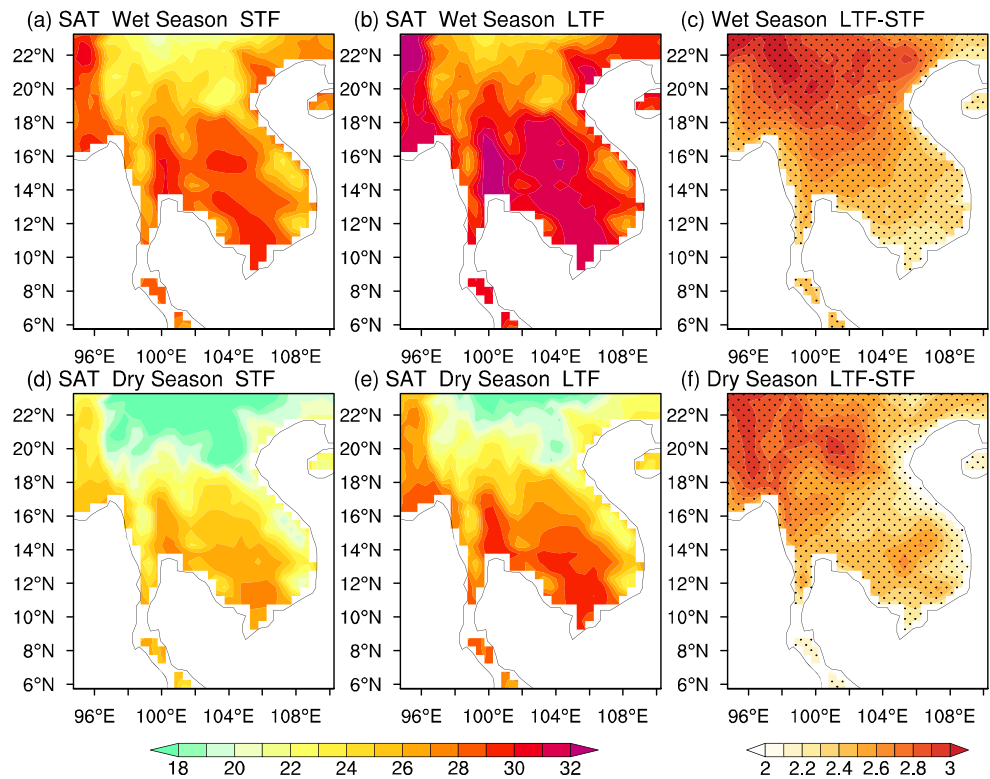


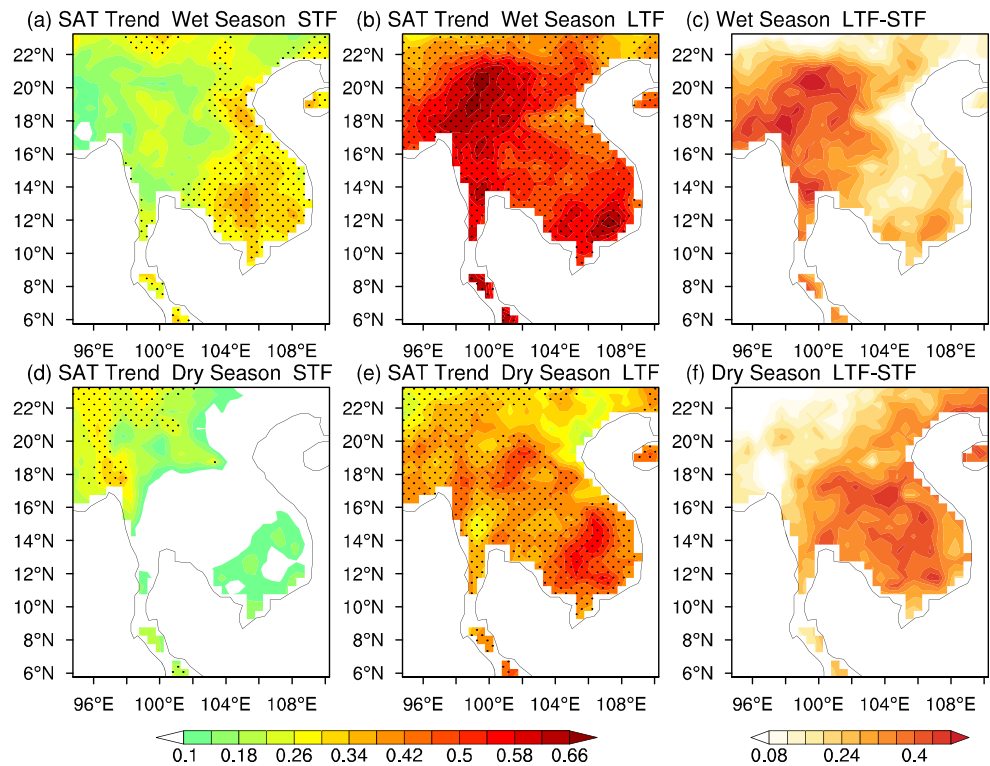
**Fig. 3** Spatial distributions of the projected seasonal mean SAT (unit: °C) over the ICP under the RCP 8.5 for the short-term future (a, d) and the long-term future (b, e), as well as the differences between the short- and long-term future (c, f). The black dots indicate statistical significance at the 95% confidence level



season, respectively. That is, the averaged SAT increases by 2.61 °C in the wet season from short- to long-term future, which is slightly faster than 2.50 °C in the dry season. The

differences in the projected SAT between the short- and long-term future show similar distributions for wet (Fig. 3c) and dry (Fig. 3f) seasons. The most conspicuous warming from short-

**Fig. 4** Spatial distributions of the projected trends of seasonal mean SAT (unit: °C decade<sup>-1</sup>) over the ICP under the RCP 8.5 for the short-term future (a, d) and the long-term future (b, e), as well as the differences between the short- and long-term future (c, f). The black dots indicate statistical significance at the 90% confidence level



to long-term future happens in the northwestern part of ICP in both seasons.

Projected spatial distributions of the seasonal SAT trends of short- and long-term future show SAT with positive trends in both wet and dry seasons under the RCP 8.5. However, the trend magnitudes differ considerably between the two seasons and the two periods: from the short- to long-term future warming intensifies. In the short-term future, the SAT trend patterns of the two seasons are reversed, with the significantly largest trends occurring over the southeast ICP in the wet season (Fig. 4a) and over the northwest in the dry season (Fig. 4d). For the long-term future, the rapid warming is strengthening significantly (at the 90% significance level) over the whole ICP for both seasons (Fig. 4b, e). From the short- to long-term future, most noticeable is the regional SAT seasonal trend increasing in the northwestern part of the ICP in the wet (Fig. 4c) and in the south ICP in the dry season (Fig. 4f).

Moreover, the wet season during the short-term future is characterized by a larger SAT trend of  $0.22\text{ }^{\circ}\text{C decade}^{-1}$  (Table 2) compared with the dry season with the warming rate of  $0.11\text{ }^{\circ}\text{C decade}^{-1}$ . During the long-term future, the respective trends are  $0.51\text{ }^{\circ}\text{C decade}^{-1}$  and  $0.42\text{ }^{\circ}\text{C decade}^{-1}$  for wet and dry seasons. However, the increasing trend is not statistically significant in the dry season during the short-term future, whereas it passes the 90% significance level for the other cases.

It can be concluded that SAT is changing in wet and dry seasons during short- and long-term future, but it differs in different seasons for both periods with generally larger trends in the wet season during the long-term future. The attribution of variations to the forcing is discussed in the following subsection.

### 3.3 The forcing impacts on the SAT variations

To investigate the possible mechanism of the SAT warming variations over the ICP under the RCP 8.5 scenario, the radiative forcing is analyzed, including aspects of the cloud cover, the downward longwave radiation, and the atmospheric water vapor content. The recent global surface temperature

warming, which is predominantly modulated by the Earth's radiation budget, has been attributed to the changing atmospheric composition caused by the anthropogenic activities, perturbing the radiation balance of the Earth (Fasullo and Trenberth 2008a, b; Knutti and Hegerl 2008; Trenberth and Fasullo 2010).

The surface net radiation can be formulated as:

$$E_0^* = E_{1,0}^* + E_{s,0}^*$$

with the net longwave and net shortwave radiation,  $E_{1,0}^* = E_{1,0}^{\downarrow} - E_{1,0}^{\uparrow}$  and  $E_{s,0}^* = E_{s,0}^{\downarrow} - E_{s,0}^{\uparrow}$ , where  $E_{1,0}^*$  is the terrestrial upward longwave radiation and  $E_{1,0}^{\downarrow}$  is the atmospheric downward longwave radiation directed to the surface and  $E_{1,0}^{\uparrow}$  is the upward longwave radiation from the Earth's surface;  $E_{s,0}^*$  is the net shortwave radiation at the surface,  $E_{s,0}^{\downarrow}$  is the incoming, and  $E_{s,0}^{\uparrow}$  the reflected radiation at the surface.

The cloud cover and radiation variations are closely associated with SAT changes. With respect to warming, clouds act in three ways, which make their overall effect so complex: (i) a “mirror” reflecting incident sunlight; (ii) a “blanket (or insulator)” trapping the heat on the planet; and (iii) a “radiator” releasing heat into space. Whether a cloud acts more like a “mirror,” “blanket,” or “radiator” depends on which level in the atmosphere (temperature) they act and on their composition of ice or water, and these three factors may cancel each other. For instance, the increased (mostly low) cloud cover would reduce the surface incoming shortwave radiation cooling the surface. The cooling effect of clouds is partially offset by cooler (higher) clouds reducing the emission into space by absorbing the heat emitted from the surface and re-radiating part of it, thus acting like a “blanket” and, thereby, reducing the cooling rate at the surface. On the other hand, the surface temperature may even be increased by the “blanket” effect of high-level clouds enhancing downward longwave radiation and reducing shortwave reflection. Also, the effect of cloud thickness plays a non-negligible role in a real world but is not considered here.

**Table 2** Statistical trends of the seasonal surface air temperature (unit:  $^{\circ}\text{C decade}^{-1}$ ), cloud cover (unit: fraction  $\text{decade}^{-1}$ ), vertically integrated specific humidity (unit:  $\text{kg m}^{-2} \text{decade}^{-1}$ ), and downward longwave

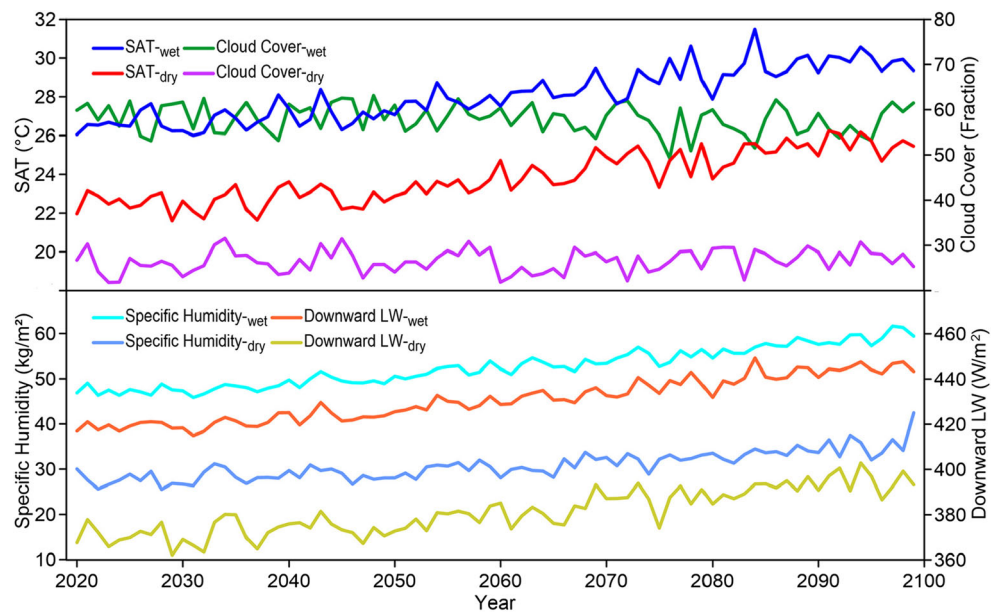
radiation (unit:  $\text{W m}^{-2} \text{decade}^{-1}$ ) over the ICP for the short-term future (STF) and the long-term future (LTF)

Season	Surface air temperature		Cloud cover		Vertically integrated specific humidity		Downward longwave radiation	
	STF	LTF	STF	LTF	STF	LTF	STF	LTF
Wet	0.22*	0.51**	0.48	-0.18	1.03**	2.17**	2.12**	4.46**
Dry	0.11	0.42**	0.46	0.50	0.43	1.45**	1.49	3.67**

\*Statistical significance at the 90% confidence level

\*\*Statistical significance at the 95% confidence level

**Fig. 5** Time series of the seasonal mean SAT, cloud cover, vertically integrated specific humidity, and the downward longwave radiation averaged over the ICP under the RCP 8.5 scenario for the period of 2020–2099



The variations of the annual mean SAT, cloud cover, the downward longwave radiation, and the vertically integrated specific humidity under the RCP 8.5 scenario during 2020–2099 are presented in Fig. 5. While downward longwave radiation and specific humidity increase in the RCP 8.5 projection, resembling the SAT variation, the cloud cover fluctuations remain relatively moderate. For both wet and dry seasons, the cloud cover variations do not reveal significant changes or large discrepancies (Table 2), while the downward longwave radiation is significantly correlated (0.97) with SAT. Furthermore, the water vapor content and the downward longwave radiation are significantly correlated by 0.97 and 0.77 for wet and dry seasons. That is, the continuously increasing vertically integrated specific humidity (following the Clausius-Clapeyron relation) leads to a constantly rising atmospheric longwave counter radiation, which ultimately is responsible for the surface temperature change (Ruckstuhl et al. 2007).

Trends of cloud cover, specific humidity, and downward longwave radiation during the short- and long-term future are further determined for wet and dry seasons. The cloud cover shows non-significant changing rates for both seasons in the short- and long-term future, while the vertically integrated specific humidity increases in the wet season ( $1.03 \text{ kg m}^{-1} \text{ decade}^{-1}$  and  $2.17 \text{ kg m}^{-1} \text{ decade}^{-1}$ ) passing the 95% significance test for the short- and long-term future, respectively. In the dry season, the change is non-significant ( $0.43 \text{ kg m}^{-1} \text{ decade}^{-1}$ ) for the short-term future but significant ( $1.45 \text{ kg m}^{-1} \text{ decade}^{-1}$ ) for the long-term future. The water vapor content of the atmosphere rises more sharply in the wet season during the long-term future. Subsequently, the downward longwave radiation is characterized by similar trend patterns (Table 2).

In summary, these results suggest that cloud cover appears to have no net effect on the SAT warming over the ICP during

2020–2099, while, independent of the atmospheric  $\text{CO}_2$  content, they determine the accuracy/sensitivity of the response. The next generation of models used for the future IPCC reports may allow evaluations with more details. The higher  $\text{CO}_2$  concentrations in the long-term future under the RCP 8.5 scenario increase the downward longwave radiation (Fig. 5), which consequently enhances the atmospheric greenhouse effect and further heat up the near-surface air. The consideration is that the maximum amount of water vapor that can be dissolved in air increases rapidly with temperature, especially in the wet season, in accordance with the Clausius-Clapeyron relation. With respect to the study area of the ICP, the great temperature sensitivity to fluctuations in longwave radiation can be attributed to a strong positive feedback from the increasing water vapor (Hense et al. 1988; Flohn et al. 1992; Folland et al. 2002), which also has a greenhouse effect (Rodhe 1990) and in turn results from the heating due to increased concentrations of anthropogenic gases radiatively active in the longwave spectrum (Stanhill 2011). Due to the effect of the atmospheric counter radiation, the SAT increases rapidly and adjusts to a new equilibrium state.

## 4 Conclusion and discussion

Increasing concerns about climate change have been specifically addressed in the regions and countries surrounding the Indochina Peninsula (ICP). Given the considerable capability of the regionally coupled atmosphere-ocean model ROM, which includes exchanges of momentum, heat, and water fluxes between the atmosphere (REMO) and ocean (MPIOM) models, the projected seasonal surface air temperature (SAT) changes over the ICP under the Representative Concentration Pathway (RCP) 8.5 scenario and the possible

mechanisms are analyzed for the short-term future (2020–2049) and the long-term future (2070–2099), with the following results obtained.

- (i) Projected SAT distributions exhibit similar patterns for wet and dry seasons in the short- and long-term future, with the highest SAT located in the southern coastal area and the lowest SAT in the northern mountainous area of the ICP. The regionally averaged SAT over the ICP increases by 2.61 °C in the wet season from short- to long-term future, which is slightly higher than that of 2.50 °C in the dry season. Besides, the differences in the projected SAT between the short- and long-term future show similar distributions for the two seasons, with the most conspicuous warming located in the northwestern part of the ICP.
- (ii) During the short-term future, the SAT trends show patterns reversing between the two seasons, with the largest trends occurring over the southeast and northwest ICP in wet and dry seasons, respectively. The regionally averaged warming rates are 0.22 °C decade<sup>-1</sup> and 0.11 °C decade<sup>-1</sup> in wet and dry seasons, but not statistically significant in the dry season. As for the long-term future, the rapid warming is strengthened significantly over the whole ICP in the two seasons, with corresponding trends of 0.51 °C decade<sup>-1</sup> and 0.42 °C decade<sup>-1</sup>, both passing the 90% significance level. The most noticeable increasing magnitudes are located over the northwest ICP in the wet season and over the south ICP in the dry season.
- (iii) Cloud cover variations do not exhibit a significant net influence on the SAT warming over the ICP during 2020–2099. In the long-term future under the RCP 8.5 scenario, higher CO<sub>2</sub> concentrations lead to increasing downward longwave radiation, which enhances the greenhouse effect of the atmosphere. The intensified warming could be mainly attributed to the intensified impact of the atmospheric counter radiation. Additionally, the water vapor content of the atmosphere and the counter radiation are interacted by a positive feedback process, which in turn strengthens the SAT warming, especially in the wet season.

The regionally coupled model ROM is preliminarily employed with a fairly fine scale to obtain a general impression of the future SAT changes over the ICP and the corresponding underlying forcing controls under the RCP 8.5 scenario, which can be considered a complementation of previous studies on regional climate projections. However, although the ROM model reasonably represents many aspects of the regional climate, some biases persist and leave potential for future improvements. The cloud cover in ROM is currently simulated using a single-layer cloud cover without distinguishing low-, mid-, and high-level clouds. Therefore, the impacts of clouds at different levels on the regional climate change require further research.

Among the emissions assumed by scientists for the future climate, the business-as-usual scenario of RCP 8.5 corresponds to the high population growth and energy consumption without climate mitigation strategies and represents a high-risk future climate that some researchers consider to be the least realistic in the long term (Hausfather and Peters 2020). However, reports also suggest that the most severe of the available climate change scenarios, i.e., RCP 8.5, could still underestimate the impact of emission concentrations (Christensen et al. 2018). It may not adequately account for the real warming rates considering the carbon feedback processes (Schaefer et al. 2014; Lenton et al. 2019). In the context of the strengthening global warming (IPCC 2018; Forster et al. 2020; Zhu et al. 2020a), such a “worst-case” scenario of RCP 8.5 is applied to estimate the extreme outcomes and potential threats of the worst-case emission on the future climate change, although it might happen in an imagined world. Results of our experiment are in line with those from the state-of-the-art models in the short- and long-term future climate projections (Shiru et al. 2020; Ullah et al. 2020), which not only indicates the skillful simulation of regional climate in the ROM model but also reveals the potential forcing impacts on the local temperature variation and highlights the importance of restricting the rising global temperature. In addition, more factors such as precipitation, humidity, and atmospheric circulation need to be further investigated focusing on some specific regions under the global warming. The upper limitations of changes in future climate should also be understood in depth using the next generation of scenarios and models.

**Acknowledgments** We are grateful to Prof. Yuanfa Gong and Dr. Xiaofei Wu for inspiring discussions about radiation balance of the Earth. We would like to thank the German Climate Computing Center (DKRZ) for their resources.

**Funding information** The authors received joint financial support from the National Natural Science Foundation of China (41805056, 41776002, 41875102, and 41875169), the National Key R&D Program of China (2017YFC1502002, 2018YFC1505702, and 2018YFC1506104), the Application and Basic Research of Sichuan Department of Science and Technology (2019YJ0316), the Sichuan Science and Technology Program (2020JDJQ0050), the Postgraduate Research & Practice Innovation Program of Jiangsu Province (KYCX17\_0875), the Scientific Research Foundation of Chengdu University of Information Technology (KYTZ201730), the Project Supported by Scientific Research Fund of Sichuan Provincial Education Department (18ZB0112), the Open Research Fund Program of KLME, NUIST (KLME201809), and the China Scholarship Council (201608320193 and 201808510009).

## References

- Aldrian E, Sein D, Jacob D, Gates LD, Podzun R (2005) Modelling Indonesian rainfall with a coupled regional model. *Clim Dyn* 25: 1–17



- Cabos W, Sein DV, Pinto JG, Fink AH, Koldunov NV, Alvarez F, Izquierdo A, Keenlyside N, Jacob D (2017) The South Atlantic Anticyclone as a key player for the representation of the tropical Atlantic climate in coupled climate models. *Clim Dyn* 48:4051–4069
- Cabos W, Sein DV, Durán-Quesada A, Liguori G, Koldunov NV, Martínez-López B, Alvarez F, Sieck K, Limareva N, Pinto JG (2019) Dynamical downscaling of historical climate over CORDEX Central America domain with a regionally coupled atmosphere-ocean model. *Clim Dyn* 52:4305–4328
- Christensen P, Gillingham K, Nordhaus W (2018) Uncertainty in forecasts of long-run economic growth. *Proc Natl Acad Sci U.S.A* 115: 5409–5414
- Fasullo JT, Trenberth KE (2008a) The annual cycle of the energy budget: Pt I. Global mean and land-ocean exchanges. *J Clim* 21:2297–2313
- Fasullo JT, Trenberth KE (2008b) The annual cycle of the energy budget: Pt II. Meridional structures and poleward transports. *J Clim* 21: 2314–2326
- Feser F, Rockel B, von Storch H, Winterfeldt J, Zahn M (2011) Regional climate models add value to global model data: a review and selected examples. *Bull Am Meteorol Soc* 92:1181–1192
- Flohn H, Kapala A, Knoche HR et al (1992) Water vapor as an amplifier of the greenhouse effect: new aspects. *Meteorol Zeitschrift* 1:122–138
- Folland CK, Karl TR, Salinger MJ (2002) Observed climate variability and change. *Weather* 57:269–278
- Forster PM, Maycock AC, McKenna CM, Smith CJ (2020) Latest climate models confirm need for urgent mitigation. *Nat Clim Chang* 10:7–10
- Gaertner MA, González-Alemán JJ, Romera R, Domínguez M, Gil V, Sánchez E, Gallardo C, Miglietta MM, Walsh KJE, Sein DV, Somot S, Dell'Aquila A, Teichmann C, Ahrens B, Buonomo E, Colette A, Bastin S, van Meijgaard E, Nikulin G (2018) Simulation of medicanes over the Mediterranean Sea in a regional climate model ensemble: impact of ocean-atmosphere coupling and increased resolution. *Clim Dyn* 51:1041–1057
- Ge F, Zhi X, Babar ZA, Tang W, Chen P (2017) Interannual variability of summer monsoon precipitation over the Indochina Peninsula in association with ENSO. *Theor Appl Climatol* 128:523–531
- Ge F, Peng T, Fraedrich K, Sielmann F, Zhu X, Zhi X, Liu X, Tang W, Zhao P (2019a) Assessment of trends and variability in surface air temperature on multiple high-resolution datasets over the Indochina Peninsula. *Theor Appl Climatol* 135:1609–1627
- Ge F, Zhu S, Peng T et al (2019b) Risks of precipitation extremes over Southeast Asia: does 1.5°C or 2°C global warming make a difference? *Environ Res Lett* 14:044015
- Giorgi F (2006) Regional climate modeling: status and perspectives. *J Phys IV France* 139:101–118
- Giorgi F, Jones C, Asrar GR (2009) Addressing climate information needs at the regional level: the CORDEX framework. *World Meteorol Organ (WMO) Bull* 58:175–183
- Hagemann S, Dümenil L (1997) A parametrization of the lateral waterflow for the global scale. *Clim Dyn* 14:17–31
- Hagemann S, Gates LD (2001) Validation of the hydrological cycle of ECMWF and NCEP reanalyses using the MPI hydrological discharge model. *J Geophys Res* 106:1503–1510
- Hausfather Z, Peters GP (2020) Emissions-the 'business as usual' story is misleading. *Nature* 577:618–620
- Hense A, Krahe P, Flohn H (1988) Recent fluctuations of tropospheric temperature and water vapor content in the tropics. *Meteorog Atmos Phys* 38:215–227
- Holden PG, Edwards NR, Ridgwell A et al (2018) Climate-carbon cycle uncertainties and the Paris Agreement. *Nat Clim Chang* 8:609–613
- Hsu HH, Zhou T, Matsumoto J (2014) East Asian, Indochina and western North Pacific summer monsoon-an update. *Asia-Pac J Atmos Sci* 50:45–68
- IPCC (2013) Summary for policymakers. In: climate change 2013: the physical science basis. Contribution of working group I to the Fifth Assessment Report of the Intergovernmental Panel on Climate Change. Cambridge University Press, Cambridge
- IPCC (2014) Climate change 2014: impacts, adaptation, and vulnerability. Part B: regional aspects. Contribution of working group II to the Fifth Assessment Report of the Intergovernmental Panel on Climate Change. Cambridge University Press, Cambridge
- IPCC (2018) Global warming of 1.5 °C, an IPCC special report on the impacts of global warming of 1.5°C above pre-industrial levels and related global greenhouse gas emission pathways, in the context of strengthening the global response to the threat of climate change, sustainable development, and efforts to eradicate poverty. World Meteorological Organization Geneva
- Jacob D (2001) A note to the simulation of the annual and inter-annual variability of the water budget over the Baltic Sea drainage basin. *Meteorog Atmos Phys* 77:61–73
- Jacob D, Van den Hurk B, Andrae U et al (2001) A comprehensive model inter-comparison study investigating the water budget during the BALTEX-PIDCAP period. *Meteorog Atmos Phys* 77:19–43
- Jungclaus JH, Fischer N, Haak H, Lohmann K, Marotzke J, Matei D, Mikolajewicz U, Notz D, von Storch JS (2013) Characteristics of the ocean simulations in the Max Planck Institute Ocean Model (MPIOM) the ocean component of the MPI-Earth system model. *J Adv Model Earth Syst* 5:422–446
- Karl TR, Easterling DR (1999) Climate extremes: selected review and future research directions. *Clim Chang* 42:309–325
- Kendall MG (1975) Rank correlation methods, 4th edn. Charles Griffin, London
- Knutti R, Hegerl GC (2008) The equilibrium sensitivity of the Earth's temperature to radiation changes. *Nat Geosci* 1:735–743
- Lenton TM, Rockström J, Gaffney O, Rahmstorf S, Richardson K, Steffen W, Schellnhuber HJ (2019) Climate tipping points-too risky to bet against. *Nature* 575:592–595
- Mann HB (1945) Nonparametric tests against trend. *Econometrica J Econ Soc* 13:245–259
- Manton MJ, Della-Marta PM, Haylock MR, Hennessy KJ, Nicholls N, Chambers LE, Collins DA, Daw G, Finet A, Gunawan D, Inape K, Isobe H, Kestin TS, Lefale P, Leyu CH, Lwin T, Maitrepierre L, Ouprasitwong N, Page CM, Pahalad J, Plummer N, Salinger MJ, Suppiah R, Tran VL, Trewin B, Tibig I, Yee D (2001) Trends in extreme daily rainfall and temperature in Southeast Asia and the South Pacific: 1961-1998. *Int J Climatol* 21:269–284
- Marsland SJ, Haak H, Jungclaus JH, Latif M, Röske F (2003) The Max-Planck-Institute global ocean/sea ice model with orthogonal curvilinear coordinates. *Ocean Model* 5:91–127
- Meehl GA, Covey C, Taylor KE et al (2007) The WCRP CMIP3 multimodel dataset: a new era in climate change research. *Bull Am Meteorol Soc* 88:1383–1394
- Moss RH, Edmonds JA, Hibbard KA, Manning MR, Rose SK, van Vuuren DP, Carter TR, Emori S, Kainuma M, Kram T, Meehl GA, Mitchell JFB, Nakicenovic N, Riahi K, Smith SJ, Stouffer RJ, Thomson AM, Weyant JP, Wilbanks TJ (2010) The next generation of scenarios for climate change research and assessment. *Nature* 463:747–756
- Ngo-Duc T, Tangang FT, Santisirisomboon J, Cruz F, Trinh-Tuan L, Nguyen-Xuan T, Phan-Van T, Juneng L, Narisma G, Singhruck P, Gunawan D, Aldrian E (2017) Performance evaluation of RegCM4 in simulating extreme rainfall and temperature indices over the CORDEX-Southeast Asia Region. *Int J Climatol* 37:1634–1647
- Riahi K, Rao S, Krey V, Cho C, Chirkov V, Fischer G, Kindermann G, Nakicenovic N, Rafaj P (2011) RCP 8.5 - a scenario of comparatively high greenhouse gas emissions. *Clim Chang* 109:33–57
- Rodhe H (1990) A comparison of the contribution of various gases to the greenhouse effect. *Science* 248:1217–1219

- Ruckstuhl C, Philipona R, Morland J et al (2007) Observed relationship between surface specific humidity, integrated water vapor, and longwave downward radiation at different latitudes. *J Geophys Res* 112:D03302
- Schaefer K, Lantuit H, Romanovsky VE, Schuur EAG, Witt R (2014) The impact of the permafrost carbon feedback on global climate. *Environ Res Lett* 9:085003
- Schleussner CF, Lissner TK, Fischer EM, Wohland J, Perrette M, Golly A, Rogelj J, Childers K, Schewe J, Frieler K, Mengel M, Hare W, Schaeffer M (2016) Differential climate impacts for policy-relevant limits to global warming: the case of 1.5°C and 2°C. *Earth Syst Dyn* 7:327–351
- Sein DV, Koldunov NV, Pinto JG, Cabos W (2014) Sensitivity of simulated regional Arctic climate to the choice of coupled model domain. *Tellus A* 66:23966
- Sein DV, Mikolajewicz U, Gröger M, Fast I, Cabos W, Pinto JG, Hagemann S, Semmler T, Izquierdo A, Jacob D (2015) Regionally coupled atmosphere-ocean-sea ice-marine biogeochemistry model ROM: 1. Description and validation. *J Adv Model Earth Syst* 7:268–304
- Sen PK (1968) Estimates of the regression coefficient based on Kendall's tau. *J Am Stat Assoc* 63:1379–1389
- Shiru MS, Chung ES, Shahid S, Alias N (2020) GCM selection and temperature projection of Nigeria under different RCPs of the CMIP5 GCMS. *Theor Appl Climatol* 141:1611–1627
- Stanhill G (2011) The role of water vapor and solar radiation in determining temperature changes and trends measured at Armagh, 1881–2000. *J Geophys Res* 116:D03105
- Steele M, Morley R, Ermold W (2001) PHC: a global ocean hydrography with a high-quality Arctic Ocean. *J Clim* 14:2079–2087
- Takahashi HG, Yasunari T (2006) A climatological monsoon break in rainfall over Indochina - a singularity in the seasonal march of the Asian summer monsoon. *J Clim* 19:1545–1556
- Tangang FT, Juneng L, Ahmad S (2007) Trend and interannual variability of temperature in Malaysia: 1961–2002. *Theor Appl Climatol* 89:127–141
- Tao H, Gemmer M, Bai Y, Su B, Mao W (2011) Trends of streamflow in the Tarim River Basin during the past 50years: human impact or climate change? *J Hydrol* 400:1–9
- Taylor KE, Stouffer RJ, Meehl GA (2012) An overview of CMIP5 and the experiment design. *Bull Am Meteorol Soc* 93:485–498
- Trenberth KE, Fasullo JT (2010) Tracking earth's energy. *Science* 328:316–317
- Ullah S, You Q, Zhang Y et al (2020) Evaluation of CMIP5 models and projected changes in temperature over South Asia under global warming of 1.5 °C, 2 °C, and 3 °C. *Atmos Res* 246:105122
- UNFCCC (2015) Adoption of the Paris Agreement. I: proposal by the President (Draft Decision). United Nations Office, Geneva
- Valcke S, Caubel A, Declat D et al (2003) Oasis3 ocean atmosphere sea ice soil user's guide. CERFACS, Toulouse
- Villafuerte MQ, Matsumoto J (2015) Significant influences of global mean temperature and ENSO on extreme rainfall in Southeast Asia. *J Clim* 28:1905–1919
- You Q, Fraedrich K, Ren G, Pepin N, Kang S (2013) Variability of temperature in the Tibetan Plateau based on homogenized surface stations and reanalysis data. *Int J Climatol* 33:1337–1347
- You Q, Min J, Zhang W, Pepin N, Kang S (2015) Comparison of multiple datasets with gridded precipitation observations over the Tibetan Plateau. *Clim Dyn* 45:791–806
- Yue S, Hashino M (2003) Temperature trends in Japan: 1900–1996. *Theor Appl Climatol* 75:15–27
- Zhu X, Bye J, Fraedrich K, Bordi I (2016) Statistical structure of intrinsic climate variability under global warming. *J Clim* 29:5935–5947
- Zhu S, Ge F, Fan Y, Zhang L, Sielmann F, Fraedrich K, Zhi X (2020a) Conspicuous temperature extremes over Southeast Asia: seasonal variations under 1.5 °C and 2 °C global warming. *Clim Chang* 160:343–360
- Zhu S, Remedio ARC, Sein D et al (2020b) Added value of the regionally coupled model ROM in the East Asian summer monsoon modeling. *Theor Appl Climatol* 140:375–387

**Publisher's note** Springer Nature remains neutral with regard to jurisdictional claims in published maps and institutional affiliations.